Solar Phys (2013) 288:369–387
DOI 10.1007/s11207-013-0296-6

Velocity-Space Proton Diffusion in the Solar Wind Turbulence

Y. Voitenko · V. Pierrard

Received: 15 July 2012 / Accepted: 2 April 2013 / Published online: 7 May 2013

Abstract We study the velocity-space quasi-linear diffusion of the solar wind protons driven by oblique Alfvén turbulence at proton kinetic scales. Turbulent fluctuations at these scales possess the properties of kinetic Alfvén waves (KAWs) that are efficient in Cherenkov-resonant interactions. The proton diffusion proceeds via Cherenkov kicks and forms a quasi-linear plateau – the nonthermal proton tail in the velocity distribution function (VDF). The tails extend in velocity space along the mean magnetic field from 1 to $(1.5-3)\ V_{\rm A}$, depending on the spectral break position, on the turbulence amplitude at the spectral break, and on the spectral slope after the break. The most favorable conditions for the tail generation occur in the regions where the proton thermal and Alfvén velocities are about equal, $V_{\rm Tp}/V_{\rm A} \approx 1$. The estimated formation times are within 1 – 2 h for typical tails at 1 AU, which is much shorter than the solar wind expansion time. Our results suggest that the nonthermal proton tails, observed in situ at all heliocentric distances > 0.3 AU, are formed locally in the solar wind by the KAW turbulence. We also suggest that the bump-on-tail features – proton beams, often seen in the proton VDFs, can be formed at a later evolutional stage of the nonthermal tails by the time-of-flight effects.

Keywords Solar wind · Space Plasmas · Turbulence · Waves

1. Introduction

The low collisionality of the solar wind and the persistent activity of waves and turbulence make kinetic wave-particle interactions unavoidable in the solar wind modeling. The need

Y. Voitenko (✉) · V. Pierrard
Solar-Terrestrial Centre of Excellence, Space Physics Division, Belgian Institute for Space Aeronomy, Ringlaan-3-Avenue Circulaire, 1180 Brussels, Belgium
e-mail: yuriy.voitenko@oma.be

V. Pierrard
Georges Lemaître Centre for Earth and Climate Research (TECLIM), Université Catholique de Louvain, Place Louis Pasteur 3, bte L4.03.08, 1348 Louvain-la-Neuve, Belgium

for such kinetics has been emphasized in view of the numerous nonthermal features observed in velocity distribution functions (VDFs) of the solar wind particles (see Marsch (2006) and references therein). In particular, nonthermal tails, beams, and temperature anisotropies are routinely observed in situ by satellites.

Recent in situ measurements have revealed that the solar wind turbulence at proton kinetic scales is dominated by Alfvénic waves (AWs) and not by the fast mode or whistler waves (He *et al.*, 2011, 2012; Podesta and Gary, 2011). Furthermore, 80 % of the Alfvén wave energy are found in oblique quasi-perpendicular AWs, while the remaining 20 % are found in quasi-parallel ion-cyclotron Alfvén waves (ICAW) (He *et al.*, 2011).

The properties of quasi-parallel ICAWs are much better understood than that of the oblique AWs at proton kinetic scales. ICAWs experience strong ion-cyclotron resonances and are considered to be the main source for the perpendicular heating of the protons and heavier ions in the solar corona and solar wind (see reviews in Hollweg and Isenberg (2002), Marsch (2006) and references therein).

The properties of the dominant quasi-perpendicular AW fraction and its influence on particles VDFs are still unclear. Depending on the wavevector anisotropy $k_\perp/k_\parallel$ (perpendicular/parallel with respect to the mean magnetic field B_0), less oblique AWs at proton kinetic scales are similar to ICAWs, while more oblique AWs are kinetic Alfvén waves (KAWs). At intermediate $k_\perp/k_\parallel \approx V_A/V_{Tp}$, AWs possess mixed properties of both ICAWs and KAWs and are named ion-cyclotron KAWs – ICKAWs (Voitenko and Goossens, 2003). Since ICKAWs experience both the ion-cyclotron resonance (typical for ICAWs) and the Cherenkov resonance (typical for KAWs), they have a higher dissipation and more generation channels and can play an important role in the energy exchange between parallel and perpendicular degrees of freedom in the solar wind.

The wavevector anisotropy at proton kinetic scales has been measured by Sahraoui *et al.* (2010). For perpendicular wave numbers up to $k_\perp\rho_p \simeq 2$, the wave/proton-cyclotron frequency ratio appeared to be still low, $\omega/\Omega_p \simeq 0.1$, whereas the anisotropy is high, about $k_\perp/k_\parallel \simeq 10$, which is typical for classic KAWs. The dominant role of KAWs in the oblique AW fraction has been also supported by two independent tests performed by Salem *et al.* (2012), who simultaneously measured two polarization ratios: compressional magnetic/total magnetic and total electric/total magnetic field perturbations.

The interest in KAWs and related questions has risen recently in the context of turbulence dissipation in the solar wind and the consequent heating of plasma species (Schekochihin *et al.* (2009); Howes (2011); and references therein). Goldreich and Sridhar (1995) suggested that the MHD AW turbulence cascades along a critical balance path, which result in preferential generation of high perpendicular wavenumbers, and hence KAWs (Schekochihin *et al.*, 2009). An indirect confirmation of the critical balance was provided recently by Gogoberidze, Chapman, and Hnat (2012), who proved that the critical balance leads to the generation of the residual energy observed in the solar wind turbulence.

A solar wind model elaborating Landau damping of KAWs has predicted the electron and proton heating rates (Howes, 2011), which agree well with empirical estimates by Cranmer *et al.* (2009) at $\gtrsim 0.8$ AU. At smaller radial distances the proton heating by Landau damping appeared to be insufficient, and Howes (2011) suggested that proton cyclotron heating might be operating there. Because of the shorter inertial range, the MHD turbulence at shorter radial distances shows less anisotropic fluctuations at proton kinetic scales, which can produce the required proton heating via cyclotron resonant interaction.

A widely used assumption of the Maxwellian Landau damping can be violated in the solar wind by local deformations of VDFs of particles in resonant velocity ranges. Borovsky and Gary (2011) have demonstrated that the electron Landau damping is still strong (although not Maxwellian any more) because the relatively high collisionality of the electron

is capable of keeping their VDFs not far from Maxwellian. In contrast, the less-collisional protons experience much stronger departures from Maxwellian VDFs, which can significantly modify the proton Landau damping, or even cancel it.

Chandran *et al.* (2010) proposed another promising heating mechanism for the protons, stochastic acceleration by KAWs across B_0. This mechanism is not related to the kinetic wave-particle resonances, and is therefore not as sensitive to the local deformations of the proton VDFs.

If the turbulence at proton kinetic scales consists of the ion-cyclotron and KAW fractions, as is suggested by recent observations, both these fractions should produce their own observed signatures – specific features in the proton VDFs. The most typical observed features of the proton VDFs are (Marsch, 1991): i) nonthermal tails or even secondary peaks along the magnetic field direction in all solar wind types (fast, slow, and intermediate), and ii) total temperature anisotropies $T_{p\perp} > T_{p\parallel}$ in the fast solar wind (with anisotropic proton cores), and $T_{p\parallel} > T_{p\perp}$ in the slow (with isotropic cores) and intermediate (with both isotropic and anisotropic cores) solar winds. The parallel proton tails and beams are important contributors to the energy balance between parallel and perpendicular degrees of freedom. In the fast solar wind they reduce the total temperature anisotropy to $T_{p\perp}/T_{p\parallel} \gtrsim 1$ (and at times even reverse to $T_{p\parallel} > T_{p\perp}$) despite the strongly anisotropic cores of the proton VDFs, $T_{p\perp}^{core}/T_{p\parallel}^{core} = 2\text{–}3$ (see Figure 8.4 by Marsch, 1991). In the intermediate and slow solar wind they dominate the energy balance, making $T_{p\parallel}/T_{p\perp} > 1$. Among them, the nonthermal tails prevail (Marsch *et al.*, 1982). The secondary peaks (bump-on-tails) are less frequent and develop in the tail background mainly in the fast solar wind. Therefore the bump-on-tail seems to be a later evolution stage of the proton VDF as compared to the tail. At the same time, persistent nonthermal tails without bumps are observed at all distances, which suggest that the bumps are not necessary developing on the tails within the solar wind expansion timescale; their development is therefore somehow constrained or requires more time.

The anisotropic cores of the proton VDFs with $T_{p\perp}^{core} > T_{p\parallel}^{core}$ have been associated with the ion-cyclotron heating by ion-cyclotron resonant waves, and ICAW interaction with solar wind protons and heavier ions has been studied extensively (Hollweg and Isenberg (2002); Marsch (2006); and references therein). It was shown in particular that the ion-cyclotron pitch-angle diffusion can be responsible for the shaping and perpendicular heating of the core proton VDFs (Marsch and Tu, 2001), for the cross-field heating of heavier ions (Galinsky and Shevchenko, 2012), and also for the pitch-angle scattering of the nonthermal proton tails (Marsch and Bourouaine, 2011).

Wave mechanisms producing nonthermal proton tails and bump-on-tails (beams) in the solar wind received much less attention. The first mechanism, proposed by Tu, Wang, and Marsch (2002), relied upon the proton cyclotron-resonant diffusion driven by a specific ion-cyclotron mode supported by helium ions. Another mechanism, nonlinear proton trapping in the parallel KAW potentials, has been suggested by Voitenko and Goossens (2006). More recently, analytical (Pierrard and Voitenko, 2010) and numerical (Li *et al.*, 2010; Osmane, Hamza, and Meziane, 2010) studies have confirmed that a KAW with reasonable amplitude can produce observed proton beams in solar wind conditions.

Proton trapping and beam generation can also be produced by electrostatic waves carrying parallel electric fields. Recent simulations of the nonlinear decay of circularly polarized Alfvén waves have demonstrated that the product electrostatic waves can trap and accelerate protons along B_0, thereby creating a beam (Araneda, Marsch, and Vinas, 2008; Matteini *et al.*, 2011; Valentini, Perrone, and Veltri, 2011). Ion-acoustic waves (Araneda, Marsch, and Vinas, 2008; Matteini *et al.*, 2011) and "ion-bulk" waves (Valentini, Perrone, and Veltri, 2011) have been discussed as mediators transferring energy from AWs to plasma

particles. Alternatively, Rudakov *et al.* (2012) used a quasilinear approach to study the proton diffusion driven by a strongly dispersive KAW spectrum. This process can produce a quasilinear plateau in the form of a nonthermal tail in the proton VDF.

Earlier kinetic models of the solar wind electrons, accounting for the influence of external macroscopic forces and Coulomb collisions (Pierrard, Maksimovic, and Lemaire, 1999; Lie-Svendsen and Leer, 2000; Vocks and Mann, 2009), have been recently improved by including terms that account for whistler turbulence (Pierrard, Lazar, and Schlickeiser, 2011). It was concluded that the whistler turbulence, if it exists in the solar wind, could lead to the velocity-space diffusion of electrons and form nonthermal tails in the electron VDF. Another source for the velocity-space electron diffusion has been studied by Rudakov *et al.* (2011), who assumed a spectrum of kinetic Alfvén waves (KAWs) instead of whistlers. Moreover, Rudakov *et al.* (2011) argued that the nonlinear KAW scattering off electrons is more efficient than the nonlinear wave-wave interaction in the short-wavelength KAW range.

In the present paper we study the influence of the observed kinetic-scale turbulence on the evolution of the proton VDF. First we derive the Fokker–Planck diffusion terms for protons under the action of Alfvénic turbulence. We are interested here in the influence of the KAW component, which is dominant in the kinetic-scale solar wind turbulence, on the evolution of the proton VDF. The Fokker–Planck diffusion coefficients are presented in terms of quantities measured in situ in the solar wind. In particular, we refer to magnetic-field measurements that provided spectral indexes of the solar wind turbulence at proton kinetic scales (Alexandrova *et al.*, 2009; Sahraoui *et al.*, 2010), MHD/kinetic spectral break wavenumber, and the turbulence amplitude at the break wavenumber (Smith *et al.*, 2006; Markovskii, Vasquez, and Smith, 2008). Analytical and numerical estimations are given for the evolution of nonthermal tails in the proton VDFs.

2. Wave Model

The classic KAW dispersion can be presented as

$$\omega_k = k_\parallel V_\mathrm{A} K, \tag{1}$$

where $\mathbf{k}$ is the wave vector, $\parallel(\perp)$ mean components parallel (perpendicular) to $\mathbf{B}_0$, $K = K(\mu)$ is the KAW dispersion function, and $\mu = \rho_\mathrm{p} k_\perp$ is the dimensionless perpendicular wavenumber.

The kinetic dispersion function for KAWs was derived by Hasegawa and Chen (1976):

$$K = \mu \sqrt{\frac{1}{1-\Lambda_0} + \frac{T_{\mathrm{e}\parallel}}{T_{\mathrm{p}\perp}}}, \tag{2}$$

where $\Lambda_0 = \Lambda_0(\mu) = I_0(\mu^2)\exp(-\mu^2)$, $I_0(\mu^2)$ is the zero-order modified Bessel function, and $T_{\mathrm{e}(p)}$ is the electron (proton) temperature. This expression was obtained in the following wave and plasma parameter ranges: $k_\parallel^2/k_\perp^2 \ll 1$, $\omega_k^2/\Omega_\mathrm{p}^2 \ll 1$, $V_\mathrm{Tp}^2 \ll V_\mathrm{A}^2 \lesssim (\omega_k/k_\parallel)^2 \ll V_\mathrm{Te}^2$.

The KAW dispersion function gives the KAW phase velocity, $V_k = \omega_k/k_\parallel$, in units of Alfvén velocity: $V_k/V_\mathrm{A} = K(\mu)$. In the MHD limit $\mu \to 0$ KAWs become dispersiveless Alfvén waves, $V_k \to V_\mathrm{A}$, but with growing μ the KAW phase velocity deviates from the Alfvén velocity significantly. The inverse function $K^{-1}(V_k/V_\mathrm{A})$, which we will need later in the diffusion coefficient, is impossible to find from Equation (2) analytically in a general case. Explicit expressions for $K^{-1}(V_k/V_\mathrm{A})$ can only be found in two asymptotic regimes of weak ($\mu^2 \ll 1$) and strong ($\mu^2 \gg 1$) wave dispersion.

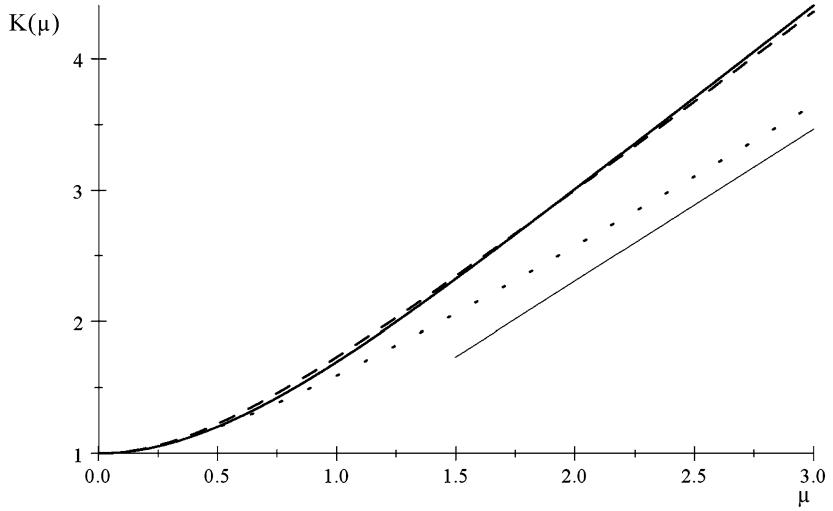

Figure 1 Comparison of three models for the KAW dispersion function $K(\mu)$: (1) kinetic dispersion by Hasegawa and Chen (1976) for $\beta \ll 1$ (solid line); (2) Padé approximation, which corresponds to the two-fluid MHD dispersion for $\beta \ll 1$ (dash line); (3) two-fluid dispersion with finite-β effects for $\beta_\parallel = \beta_\perp = 0.5$ (dotted line) and its asymptote (bottom solid line). In all cases $T_{e\parallel}/T_{p\perp} = 1$.

To simplify the problem, one can use a Padé approximation for $\Lambda_0(\mu)$,

$$\Lambda_0(\mu) \simeq \frac{1}{1+\mu^2}, \tag{3}$$

resulting in the following KAW dispersion function

$$K \simeq K_P = \sqrt{1 + \left(1 + \frac{T_{e\parallel}}{T_{p\perp}}\right)\mu^2} \tag{4}$$

and its derivative

$$\partial K_P/\partial\mu = \left(1 + \frac{T_{e\parallel}}{T_{p\perp}}\right)\frac{\mu}{K_P}. \tag{5}$$

These expressions can also be found in the framework of two-fluid MHD plasma model and provide a good approximation for KAWs in the whole range of μ if the plasma beta $\beta = (1 + T_{e\parallel}/T_{p\perp})V_{Tp}^2/V_A^2 \ll 1$. As Figure 1 shows, the difference between the kinetic KAW dispersion $K(\mu)$ (solid line) and its Padé approximation $K_P(\mu)$ (dashed line) is insignificant for $T_{e\parallel}/T_{p\perp} \approx 1$.

Finite-β effects come into play in the solar wind at 1 AU, where the typical value $\beta \approx 1$ (this corresponds to the plasma/magnetic pressure ratio ≈ 1). The KAW dispersion function K_β, accounting for the finite-β effects of magnetic and plasma compressibility (Voitenko and Goossens, 2002), can be modified for the case of anisotropic temperatures:

$$K_\beta^2 = \frac{1 + \frac{\beta_\parallel}{1+\beta_\perp} + \frac{1+T_{e\parallel}/T_{p\perp}}{1+\beta_\perp}\mu^2}{2} + \sqrt{\left(\frac{1 + \frac{\beta_\parallel}{1+\beta_\perp} + \frac{1+T_{e\parallel}/T_{p\perp}}{1+\beta_\perp}\mu^2}{2}\right)^2 - \frac{\beta_\parallel}{1+\beta_\perp}}, \tag{6}$$

where $\beta_{\parallel,\perp} = (1 + T_{e\parallel,\perp}/T_{p\parallel,\perp}) V^2_{Tp\parallel,\perp}/V^2_A$. This dispersion is also shown in Figure 1 (dotted line). The corresponding KAW wavenumber μ can be expressed via V_k explicitly,

$$\mu = \sqrt{\frac{1+\beta_\perp}{1+T_{e\parallel}/T_{p\perp}} \frac{(\frac{V_k}{V_A})^4 - (1+\frac{\beta_\parallel}{1+\beta_\perp})(\frac{V_k}{V_A})^2 + \frac{\beta_\parallel}{1+\beta_\perp}}{(\frac{V_k}{V_A})^2}}. \tag{7}$$

At large μ, the KAW dispersion (phase velocity) can be decreased significantly by the finite-β effects. In contrast, in the weakly dispersive range $\mu < 1$ moderate values such as $\beta = 0.5$ do not change the KAW dispersion significantly and can be approximated there as

$$\mu = K_P^{-1}\left(\frac{V_k}{V_A}\right) = \sqrt{\frac{(\frac{V_k}{V_A})^2 - 1}{1 + \frac{T_{e\parallel}}{T_{p\perp}}}}. \tag{8}$$

3. Proton Diffusion in the KAW Turbulence

The parallel component of the KAW electric field $E_{z\mathbf{k}}$ ($\mathbf{k} = (k_x, k_y, k_z)$ is the wave vector, $\mathbf{z} \parallel \mathbf{B}_0$) and makes KAWs efficient in Cherenkov interaction with plasma particles. Following Voitenko (1998) and Voitenko and Goossens (2003), we accounted for the proton VDF modifications under the action of KAWs in the framework of quasi-linear theory. We considered an axially symmetric (with respect to the background magnetic field $\mathbf{B}_0$) problem, where both the KAW spectrum and the particle velocity distributions are independent of the respective polar angles in the cross-field plane.

In general, the proton distribution function $F = F(\mathbf{r}, \mathbf{V}, t)$ in the solar wind obeys the Vlasov collisional equation

$$\left(\frac{\partial}{\partial t} + \mathbf{V}\cdot\frac{\partial}{\partial \mathbf{r}} + \mathbf{a}\cdot\frac{\partial}{\partial \mathbf{V}}\right) F = \left(\frac{\mathrm{d}F}{\mathrm{d}t}\right)_C + \left(\frac{\mathrm{d}F}{\mathrm{d}t}\right)_A, \tag{9}$$

where $\mathbf{r}$ and $\mathbf{V}$ are the position and velocity vectors of the protons, t is the time, and $\mathbf{a}$ is the proton acceleration under the action of the external forces: the macroscopic electric force $Ze\mathbf{E}_0$, the gravitational force $m\mathbf{g}$, and the Lorentz force $\propto \mathbf{v} \times \mathbf{B}_0$. The right-hand side represents the velocity-space proton diffusion due to Coulomb collisions, $(\mathrm{d}F/\mathrm{d}t)_C$, and due to wave-particle collisions,

$$\left(\frac{\mathrm{d}F}{\mathrm{d}t}\right)_A = \frac{\partial}{\partial V_z} D^A \frac{\partial F}{\partial V_z}.$$

In the diffusion coefficient D^A we integrate over the polar angles in the cross-$\mathbf{B}_0$ plain, implying that $|E_{z\mathbf{k}}|^2$ is axially symmetric, but we keep the dependence on the perpendicular component of the particle velocity,

$$D^A = \frac{\pi q_p^2}{2m_p^2} \sum_{\mathbf{k}} \delta(\omega_k - k_z V_z) J_0^2 |E_{z\mathbf{k}}|^2, \tag{10}$$

where the zero-order Bessel function $J_0 = J_0(k_\perp \rho_p V_\perp / V_{Tp})$ reflects the fact that the actual electric field of KAWs acting on the protons is reduced because of the averaging over their cyclotron orbits with the velocity-dependent gyroradius $V_\perp/\Omega_p = \rho_p V_\perp / V_{Tp}$. Other

notations are as follows: k_z and $k_\perp$ are the wave vector components parallel and perpendicular to B_0, $k_\perp^2 = k_x^2 + k_y^2$, $\rho_\mathrm{p} = V_\mathrm{Tp}/\Omega_\mathrm{p}$ is the proton gyroradius, $V_\mathrm{Tp} = \sqrt{T_\mathrm{p}/m_\mathrm{p}}$ thermal velocity, T_p temperature, m_p proton mass, q_p proton charge, and $\sum_\mathbf{k} = 2\pi \int \mathrm{d}k_z \int \mathrm{d}k_\perp\, k_\perp$. Dirac's delta-function $\delta(\omega_k - k_z V_z)$ follows from the resonant character of the Cherenkov wave-particle interaction.

The simplest solar wind models consider only the effects of the external forces. These models are called exospheric, and the right-hand side interaction terms in Equation (9) are neglected so that an analytic solution of the equation can be obtained (Lamy *et al.* (2003) and reference therein). Coulomb collisions make equations too complex and require numerical simulations. Expressions for the Coulomb diffusion term in the Vlasov equation for protons and results of numerical simulations accounting for Coulomb collisions are presented in Pierrard and Voitenko (2013).

Starting from Equation (10), the wave-particle diffusion term accounting for turbulence properties is derived in the next sections. We especially focus on the non-monotonous dependence of the diffusion coefficient on the parallel velocity, which follows from the non-monotonous dependence of the spectra of parallel electric fields on the KAW perpendicular wavenumber.

3.1. Fokker–Planck Diffusion Coefficient in Terms of KAW Magnetic Fields

Since the parallel electric fields $E_{z\mathbf{k}}$ in KAWs are relatively weak and difficult to measure, it is instructive to express D^A in terms of KAW magnetic fields. To this end one can use the KAW polarization relation

$$\frac{E_z}{B_\perp} = -\frac{T_{ez}}{T_{p\perp}} \frac{V_\mathrm{A}}{c} \frac{k_z}{k_\perp} \frac{\mu^2}{K}. \tag{11}$$

Then the 2D velocity-space diffusion coefficient for the protons can be reduced to the following integral in the normalized wavenumber space:

$$\begin{aligned} D^\mathrm{A} &= \pi^2 \frac{T_{ez}}{T_{p\perp}} \Omega_\mathrm{p} V_\mathrm{S}^2 \int \mathrm{d}\mu\, \delta\left(\mu - K^{-1}\right) \frac{\mu^3 J_0^2}{K^2 \partial K/\partial \mu} \frac{\int \mathrm{d}\nu\, \nu |B_{\mu\nu}|^2}{B_0^2} \\ &= \pi^2 \frac{T_{ez}}{T_{p\perp}} \Omega_\mathrm{p} V_\mathrm{S}^2 \left[\frac{\mu^3 J_0^2}{K^2 \partial K/\partial \mu} \frac{\int \mathrm{d}\nu\, \nu |B_{\mu\nu}|^2}{B_0^2} \right]_{\mu = K^{-1}}. \end{aligned} \tag{12}$$

The dimensionless parallel wavenumber $\nu = \delta_\mathrm{p} k_z$ (δ_p is the ion inertial length) is introduced in Equation (12), and the following relation for the Dirac δ-function is used,

$$\delta(K - V_z/V_\mathrm{A}) = \frac{\delta(\mu - K^{-1})}{\partial K/\partial \mu},$$

where $K^{-1} = K^{-1}(V_z/V_\mathrm{A})$ is the inverse K-function of V_z/V_A and $V_\mathrm{S} = \sqrt{T_{ez}/m_\mathrm{p}}$ is the ion-sound speed. The normalized spectral density, $|B_{\mu\nu}|^2 = \delta_\mathrm{p}^{-1} \rho_\mathrm{p}^{-2} |B_{\perp\mathbf{k}}|^2$, is defined such that $\int \mathrm{d}k_z \int \mathrm{d}k_\perp\, k_\perp |B_{\perp\mathbf{k}}|^2 = \int \mathrm{d}\nu \int \mathrm{d}\mu\, \mu |B_{\mu\nu}|^2$. Note that $|B_{\mu\nu}|^2$ has the same dimension as B_0^2.

Now we have to express the integral $\int_0^\infty \mathrm{d}\nu\, \nu |B_{\mu\nu}|^2$ in terms of the integral power at μ, $|B_\mu|^2 = \int \mathrm{d}\nu |B_{\mu\nu}|^2$. This last quantity is related to the unidirectional spectral density W_μ measured by the spacecraft: $\mu |B_\mu|^2 = W_\mu$. The perpendicular wavenumber μ is related to the measured spacecraft-frame frequency f through $\mu \sin\theta_{VB} \simeq (V_\mathrm{Tp}/V_\mathrm{SW})(f/f_\mathrm{p})$, θ_{VB} is the angle between the solar wind velocity V_SW and B_0.

In principle, an unknown spectrum of parallel wavenumbers ν contributes to the turbulence level at every particular μ. To simplify the problem, we take into account the following two facts. First, theory and observations suggest that the turbulence cascade proceeds along a path in wavenumber space that is defined by the "critical balance" between the linear and nonlinear timescales (Goldreich and Sridhar, 1995). In accordance with the critical balance condition, each μ has its own ν_μ where most of the spectral density is concentrated: $|B_{\mu\nu}|^2 = |B_\mu|^2\delta(\nu - \nu_\mu)$, where $|B_\mu|^2$ is the turbulence level at the perpendicular wavenumber μ. Second, the turbulence fluctuations are anisotropic with $k_\perp \gg k_z$. Denoting the anisotropy factor $k_z/k_\perp \equiv \alpha(k_\perp)$, the critical balance reads $\nu_\mu = \frac{V_A}{V_{Tp}}\alpha(\mu)\mu$. Hence we estimate $\int_0^\infty \mathrm{d}\nu\, \nu|B_{\mu\nu}|^2 \simeq \frac{V_A}{V_{Tp}}\alpha(\mu)\mu|B_\mu|^2 = \frac{V_A}{V_{Tp}}\alpha(\mu)W_\mu$, and

$$D^A = \pi^2\left(\frac{T_{ez}}{T_{p\perp}}\right)^{3/2}\Omega_p V_S V_A\left[\frac{\alpha(\mu)\mu^3 J_0^2}{K^2\partial K/\partial\mu}\frac{W_\mu}{B_0^2}\right]_{\mu=\mu_v}, \tag{13}$$

where $\mu_v = K^{-1}(V_z/V_A)$.

3.2. Diffusion Coefficient for Double-Kink Power-Law Turbulence Spectra

Further progress is possible if we know a particular shape of the turbulent spectrum of the Alfvénic turbulence. Numerous in situ observations indicate that the power law spectra $W_\mu \propto \mu^{-p}$ are typical in the solar wind, but the spectral index p is different in different ranges of μ. In the MHD turbulence range $\mu \le \mu_1$ the power law index $p = p_1 \simeq 1.7$, close to the Kolmogorov value. In the intermediate weakly/mildy dispersive KAW range $\mu_1 \le \mu \le 1$ the spectra are much steeper, with $p = p_2$ varying from $p_2 = 2$ to $p_2 = 4$ (Leamon *et al.*, 1999; Smith *et al.*, 2006; Sahraoui *et al.*, 2010). In the strongly dispersive KAW range, $\mu \gg 1$, the power index approaches the value $p = p_3 \simeq 2.8$ (Alexandrova *et al.*, 2009; Sahraoui *et al.*, 2010). This double-kink behavior of $p(\mu_v)$ can be modeled by the following piecewise function:

$$p = p(\mu) = p_1 + (p_2 - p_1)H(\mu - \mu_1) + (p_3 - p_2)H(\mu - \mu_2), \tag{14}$$

where $H(x)$ is the Heaviside step function, $H(x) = 0$ for $x < 0$ and $H(x) = 1$ for $x \ge 0$. The spectral break (more precisely, the first spectral kink) at $\mu_1 = 0.1-0.5$ separates MHD and (weakly/dispersive) kinetic ranges of Alfvénic turbulence. The second spectral kink, which occurs at $\mu_2 = 2-3$ (see spectra measured by Sahraoui *et al.* (2010), separates weakly and strongly dispersive KAW ranges (Voitenko and De Keyser, 2011).

With Equation (14), the measured spectral density can be written in the following general form:

$$W_\mu = W_{\mu 1}\left(\frac{\mu_2}{\mu_1}\right)^{(p_3-p_2)H(\mu-\mu_2)}\left(\frac{\mu}{\mu_1}\right)^{-(p_1+(p_2-p_1)H(\mu-\mu_1)+(p_3-p_2)H(\mu-\mu_2))}, \tag{15}$$

where $W_{\mu 1}$ is the turbulence spectral density at $\mu = \mu_1$ (note that $W_{\mu 1}$ has dimension of B_0^2). The re-normalization of the spectrum (Equation (15)) at $\mu \ge \mu_2$ ensures it is continuous through the second kink at $\mu = \mu_2$.

With Equation (15) the velocity diffusion coefficient (Equation (13)) attains the following general form:

$$D^A = \pi^2\Omega_p V_S V_A \frac{(\frac{T_{ez}}{T_{p\perp}})^{3/2}}{(1+\frac{T_{ez}}{T_{p\perp}})}\frac{\mu_1^2\alpha(\mu_v)(\frac{\mu_2}{\mu_1})^{(p_3-p_2)H(\mu_v-\mu_2)}(\frac{\mu_v}{\mu_1})^{2-p(\mu_v)}J_0^2(\mu_v\frac{V_\perp}{V_{Tp}})}{\frac{V_z}{V_A}}\frac{W_{\mu 1}}{B_0^2}, \tag{16}$$

where $\mu_v = \mu(V_k = V_\parallel)$ is the resonant KAW wavenumber defined by Equation (7) and $p(\mu_v)$ is given by Equation (14). In what follows we assume $\alpha(\mu) \simeq 0.1$ at ion kinetic scales $\mu \approx 1$ (Sahraoui *et al.*, 2010), and neglect its relatively slow variation in the resonant wavenumber range.

The diffusion due to KAWs is strongest for protons with velocities of about $V_z \simeq V_1 \gtrsim V_A$, which are Cherenkov-resonant with the spectral peak of the KAW parallel electric fields. In the plane $\perp B_0$, the diffusion is maximized for the core protons at $V_\perp \lesssim V_{Tp}$, where the reduction due to proton-cyclotron gyration is minimized. In the B_0-parallel direction, the diffusion coefficient decreases very fast as $V_z \to V_A$, and more slowly when V_z grows in a more extended velocity range from V_1 to several Alfvén velocities. These features are compatible with the physical picture of the Cherenkov resonant interaction between gyrating particles and waves with finite cross-B_0 length scales.

Since there are no positive $\mu = K^{-1}(V_z/V_A)$ for $V_z/V_A < 1$, $D^A = 0$ there (this fact reflects the absence of resonant KAWs for particles moving with sub-Alfvénic velocities $V_z/V_A < 1$). However, even sub-Alfvénic protons can be affected by the turbulence fluctuations via two effects: i) nonlinear broadening of the Cherenkov resonances, and ii) increased Coulomb diffusion of the protons at the steep VDF slope at $V_z \lesssim V_A$. The minimum velocity of the affected protons resulting from the former effect is analytically estimated below in Equation (22).

It is interesting to note that the spectral slope $p(\mu_v) < 2$ in (14) can make D^A a still increasing function of μ_v in the dissipation range between μ_1 and μ_2. This follows from the increase of the parallel electric fields in KAWs that is faster than the power-law decrease of the turbulence amplitudes. Therefore, depending on $p(\mu_v) \lessgtr 2$, the diffusion coefficient attains a maximum value at $\mu_v = \mu_1$ (with $p(\mu_v) > 2$) or at $\mu_v \lesssim \mu_2$ (with $p(\mu_v) < 2$). This behavior of the diffusion coefficient could have the important consequence that the less steep dissipation-range spectra result in longer nonthermal tails in the proton VDFs. But this can only be true for the cases where the turbulence amplitude is the same at $\mu = \mu_1$.

Indeed, as was found by Smith *et al.* (2006) in the inertial range, the higher spectral fluxes ϵ are followed by the steeper dissipation-range spectra p_2, such that $p_2 = 1.05\epsilon^{0.09}$. Applying this relation at the end of inertial range, we find the scaling

$$W_{\mu 1} \propto p_2^{7.4}, \tag{17}$$

relating the spectral power $W_{\mu 1}$ at the break $\mu = \mu_1$ and the spectral index p_2 above it. If the spectral powers in two cases (1) and (2) are $W_{\mu 1}^{(1)}$ and $W_{\mu 1}^{(2)}$, then the ratio $W_{\mu 1}^{(1)}/W_{\mu 1}^{(2)} = (p_2^{(1)}/p_2^{(2)})^{7.4}$. Elaborating this scaling relation, a reduced 1D diffusion coefficient is shown in Figure 2 for three spectral indices $p_2 = 4$, 3, and 2 from top to bottom. The reduction was performed by the averaging of J_0^2 in (16) in the cross-field velocity plane. With the correlation found by Smith *et al.* (2006), the diffusion coefficient, on average, is larger for steeper dissipation-range spectra, even if they decrease faster with V_z.

These properties of the diffusion coefficient indicate that kinetic Alfvén turbulence can be efficient in diffusing the protons in the velocity range covered by nonthermal tails of the proton VDFs. This is supported by the analytical and numerical estimations presented below.

4. Evolution of Nonthermal Tails in the Proton VDFs

We investigate here what types of nonthermal proton tails can be formed by their quasi-linear diffusion along the kinetic turbulent spectrum described above. We consider a local

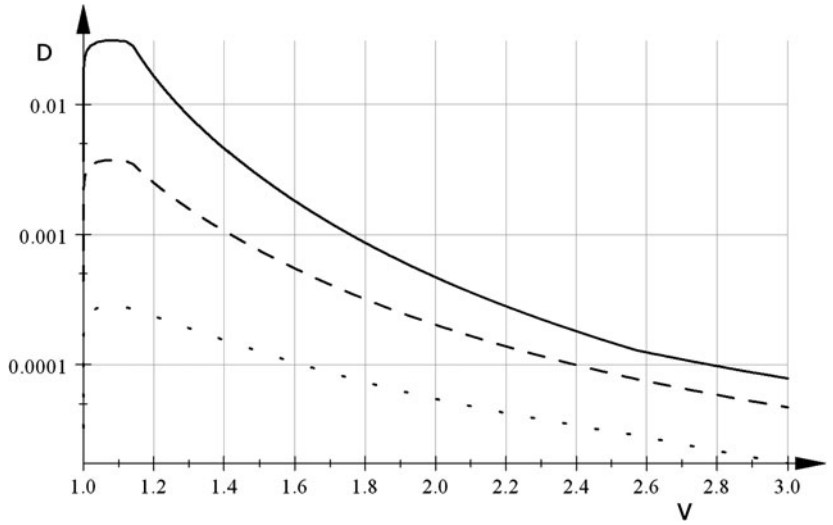

Figure 2 Reduced diffusion coefficient as function of normalized parallel velocity $V = V_z/V_A$ for $p_2 = 2$ (dotted line), $p_2 = 3$ (dashed line), and $p_2 = 4$ (solid line). The turbulence level at the first spectral kink is adjusted for each p_2 using the scaling $W_{\mu 1} \propto p^{7.4}$.

evolution problem in the solar wind neglecting the external forces, spatial variations, and Coulomb collisions in Equation (9). To estimate the formation time for a particular tail, we have to know the tail extension in the field-aligned direction V_{max}. Observations show that the tail extension V_{max} rarely exceeds $3V_A$, which allows us to simplify the problem by accounting only for the intermediate KAW spectrum in the diffusion coefficient (Equation (16)). The cross-field velocity spread in the tails is approximately the same as in the proton core, $\approx V_{Tp\perp}$ (within a multiplier of about 1).

Accounting for this, we reduce Equation (9) to the 1D diffusion equation

$$\frac{\partial f}{\partial t} = \frac{\partial}{\partial V_z} D \frac{\partial f}{\partial V_z} \tag{18}$$

for the reduced 1D distribution function $f = f(V_z) = 2\pi \int \mathrm{d}V_\perp \, V_\perp F(V_z, V_\perp)$. The 1D diffusion coefficient in the range $V_A < V_z < 3V_A$,

$$D \simeq 0.1\pi^2 \Omega_p V_S V_A \frac{(T_{ez}/T_{p\perp})^{3/2}}{(1 + T_{ez}/T_{p\perp})} \frac{\mu_1^{p_2} \Lambda_0(\mu_v^2)}{\mu_v^{p_2-2}} \frac{V_A}{V_z} \frac{W_{\mu 1}}{B_0^2}, \tag{19}$$

follows from Equation (16) after averaging over the Maxwellian distribution in the cross-field plane, $\langle J_0^2(\mu_v \frac{V_\perp}{V_{Tp}}) \rangle = \Lambda_0(\mu_v^2)$.

For small μ_1 the corresponding resonant velocity $V_1 = V_A K(\mu_1)$ is close to V_A and the remaining velocity interval $V_A < V_z < V_1$ is narrow. The detailed behavior of the diffusion coefficient D is unimportant there because D decreases fast to 0 with $V_z \to V_A$, and the nonlinear resonance broadening of KAWs with $\mu \simeq \mu_1$ is more important.

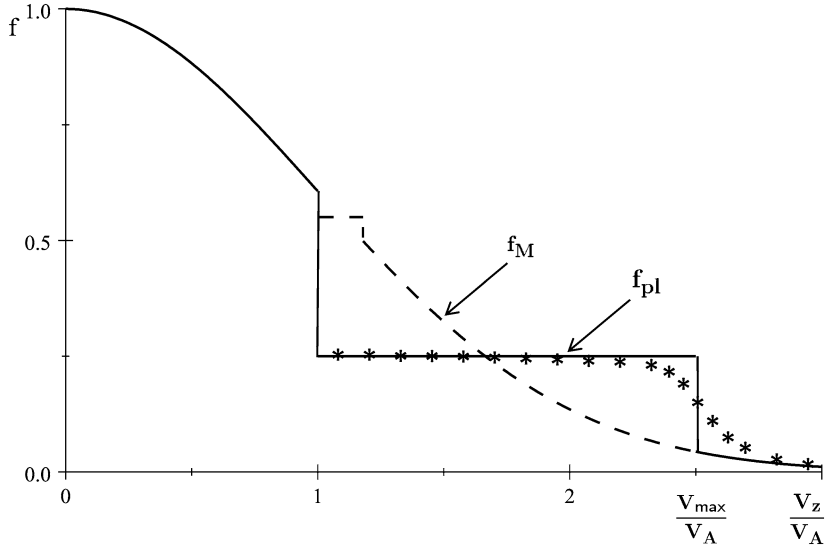

Figure 3 Model proton VDF with a step-like quasilinear plateau extending to $V_{\max} = 2.5V_A$ at the late evolutional stage (an early evolutional stage is shown by dash line). The numerical solution of the diffusion equation (Equation (18)) for the same time is shown by stars. The model and numerically calculated VDFs match well. Details on the plasma and turbulence parameters used are given in the text.

4.1. Quasilinear Plateau Model

In this section we study the quasilinear plateau evolution under the influence of the KAW turbulence. To this end we start from the initially isotropic Maxwellian VDF for the protons

$$f_{t=0} = f_M = \frac{1}{\sqrt{2\pi}V_{Tp\|}} \exp\left(-\frac{V_z^2}{2V_{Tp\|}^2}\right).$$

The diffusion coefficient (Equation (19)) and hence the velocity-space diffusion are very different, as is seen from Figure 2. The diffusion is fastest in the vicinity of V_A, where the diffusion coefficient is highest, but decreases about two orders at $3V_A$. The quasilinear saturation in this situation occurs first around this maximum, where an initial local plateau is formed, as is shown in Figure 3 (dashed line). The resulting 1D proton VDF can be modeled by the piece-wise function with the local plateau

$$f = f_{pl} = \frac{\bar{n}_{pl}}{V_{\max} - V_{\min}} \tag{20}$$

in the velocity range $V_{\min} < V_z < V_{\max}$, and f remaining Maxwellian, $f = f_M$, outside the plateau.

The quasilinear saturation spreads in time to higher velocities, shifting the plateau front $V_{\max} = V_{\max}(t)$ forward to higher velocities, as is also shown in Figure 3 (solid line). The normalized proton number density in the plateau can be expressed in terms of the error

function Erf:

$$\bar{n}_{\rm pl} = \frac{n_{\rm pl}}{n_0} = \int_{V_{\rm min}}^{V_{\rm max}} {\rm d}V_z\, f_{\rm M} = \frac{{\rm Erf}(\frac{V_{\rm max}}{\sqrt{2}V_{\rm Tp}}) - {\rm Erf}(\frac{V_{\rm min}}{\sqrt{2}V_{\rm Tp}})}{2}. \tag{21}$$

It increases with time, but the plateau height decreases.

It is important to note that the minimum velocity of the protons involved in the plateau formation, $V_{\rm min}$, can be smaller than the minimum phase velocity of resonant KAWs, $V_{\rm A}$. As follows from the nonlinear broadening of the Cherenkov resonance for a KAW with wavenumber $k_\perp$ and amplitude B_k, the minimum velocity of the affected protons is

$$\frac{V_{\rm min}}{V_{\rm A}} = \sqrt{1 + k_\perp^2 \rho_{\rm T}^2} - \sqrt{4 \frac{V_{\rm p\parallel}}{V_{\rm A}} \frac{T_{\rm e\parallel}/T_{\rm p\parallel}}{\sqrt{T_{\rm p\perp}/T_{\rm p\parallel} + T_{\rm e\parallel}/T_{\rm p\parallel}}}} \sqrt{\frac{k_\perp \rho_{\rm T}}{\sqrt{1 + k_\perp^2 \rho_{\rm T}^2}} \frac{B_k}{B_0}}. \tag{22}$$

This formula follows from the condition that the proton kinetic energy in the wave frame is equal to the KAW potential barrier. For $T_{\rm e\parallel}/T_{\rm p\parallel} = T_{\rm p\perp}/T_{\rm p\parallel} = 1$, and the typical KAW amplitude $B_k/B_0 = 0.05$ in the vicinity of the first spectral break, at $k_\perp \rho_{\rm T} = \sqrt{1 + T_{\rm e\parallel}/T_{\rm p\perp}} k_\perp \rho_{\rm p} \simeq 0.3$, the minimum velocity reduces to $V_{\rm min} \simeq 0.8 V_{\rm A}$. The modified $V_{\rm min} < V_{\rm A}$ can significantly increase the proton number density in the tail, and hence the energy in the parallel degree of freedom compared to the case $V_{\rm min} = V_{\rm A}$. On the other hand, this decrease of $V_{\rm min}$ does not much influence the evolution timescales of the tails.

4.2. Evolution Timescale of the Quasilinear Plateau

The time evolution of the plateau spreading can be found from the diffusion equation (Equation (18)) as follows. First, we note that the time derivative of $f_{\rm pl}$ can be expressed as

$$\frac{\partial f_{\rm pl}}{\partial t} = -\frac{f_{\rm pl} - f_{\rm M}(V_{\rm max})}{V_{\rm max} - V_{\rm min}} \frac{\partial V_{\rm max}}{\partial t}. \tag{23}$$

Using expression (23) in the left-hand side of the diffusion equation (Equation (18)) and then integrating it over the plateau velocity range, from $V_{\rm min} + 0$ to $V_{\rm max} + 0$, we obtain a first-order ordinary differential equation for $V_{\rm max}$ as a function of time t:

$$\big(f_{\rm pl} - f_{\rm M}(V_{\rm max})\big) \frac{{\rm d}V_{\rm max}}{{\rm d}t} = D(V_{\rm max}) \frac{\partial f_{\rm M}(V_{\rm max})}{\partial V_{\rm max}}.$$

This equation can be solved easily by separating variables and integrating from $t = 0$ to t:

$$t = V_{\rm Tp\parallel}^2 \int_{V_{\rm min}}^{V_{\rm max}} \frac{f_{\rm pl}(V'_{\rm max})/f_{\rm M}(V'_{\rm max}) - 1}{V'_{\rm max} D(V'_{\rm max})} {\rm d}V'_{\rm max}. \tag{24}$$

We estimate the plateau formation time at 1 AU, where $\Omega_{\rm p} \simeq 1\ {\rm s}^{-1}$, $T_{\rm ez}/T_{\rm p\perp} \simeq T_{\rm ez}/T_{\rm pz} \simeq 1$ and $V_{\rm A} \simeq V_{\rm Tp} \simeq 50\ {\rm km\,s}^{-1}$. With the turbulence amplitude $|B_1|/B_0 \simeq 0.05$, spectral break wavenumber $\mu_1 \simeq 0.6$, and spectral slope $p_2 = 3$ just above the break, Equation (24) gives a time of about half an hour for the formation of the quasilinear plateau with a length equal to the average tail length $V_{\rm max} = 1.75 V_{\rm A}$. Since this time is much (more than 2 orders) shorter than the solar wind expansion time $t_{\rm SW}$ (2–4 days at 1 AU), these tails can be easily generated locally by the turbulence in the solar wind.

A long tail with $V_{\max}$ reaching $2.5V_A$ is developed by the $p_2 = 2$ turbulence at $t = 14$ h, when the local approximation is still marginally applicable. The corresponding model solution is shown in Figure 3 with the solid line. Furthermore, to verify the model, we numerically solved the proton diffusion equation (Equation (18)) with the zero-gradient Neumann boundary conditions at the lower ($V_z/V_A = 1$) and upper ($V_z/V_A = 5$) boundaries. The value for the upper boundary is chosen in such a way that its variations do not affect the solution in the velocity range $V_z/V_A = 1-3$. This solution is also shown in Figure 3 by stars. A good correspondence between numerical and analytical solutions indicates that the model (Equations (20)–(24)) is sufficient for quantitative estimations of the quasilinear plateau height, length, and evolution timescale.

For the longest tails with $V_{\max} \simeq 3V_A$, the tail-formation time approaches the solar wind expansion time $t_{SW} = 2-4$ days. This means that the local analysis for these tails is inapplicable, but it does not mean that these tails cannot be formed by the turbulence. To study these tails one needs to solve a nonlocal problem incorporating radial dependencies of the solar wind plasma and turbulence characteristics (this work is in progress). Again, even for tails as long as $V_{\max} \simeq 3V_A$, the problem can be made local with slightly increased turbulence amplitudes and/or spectral break wavenumbers, for instance to $|B_1|/B_0 \simeq 0.07$ and $\mu_1 \simeq 0.8$. These variations are within the ranges of the measured values (see Figure 2 by Markovskii, Vasquez, and Smith (2008). In addition, as we will see below, the decrease of the spectral slope p_2 (with fixed amplitude B_1) has the same effect.

Since the plateau-formation time given by Equation (24) is quite a complex function of plasma and turbulence parameters, its radial dependence requires more detailed investigations using particular plasma and turbulence models. For example, with an approximately constant break frequency (constant $k_{\perp 1}$), the plateau-formation time decreases with decreasing R as, roughly, $\sim V_A \sim R$, the same as t_{SW}. In this case the locality condition can be still satisfied much closer to the Sun, where V_A is larger and hence longer tails can be generated. Several numerical estimations with reasonable plasma and turbulence parameters have shown that the tails $V_{\max} \approx 2V_A$ can be easily generated, within half an hour, at heliocentric distances as short as $R \approx 0.1$ AU, where $t_{SW} \approx 5-7$ h. The conditions are even more favorable with constant μ_1. These estimates are compatible with Helios observations of nonthermal proton tails at all distances from 0.3 to 1 AU.

Figure 4 shows the time evolution of the plateau boundary $V_{\max} = V_{\max}(t)$ in a turbulence with the spectral power $W_{f1} \simeq 0.2\ \mathrm{nT^2\,Hz^{-1}}$ at the break frequency $f_1 \simeq 0.3$ Hz. These values are well within the ranges of the measured values and close to the average ones (see Figures 1 and 2 by Markovskii, Vasquez, and Smith (2008). The five curves in Figure 4 correspond to the five different spectral slopes $p_2 = 2$, 2.5, 3, 3.5, and 4 (from top to bottom). Longer dashes indicate larger p_2, except for the solid curve with $p_2 = 3$. Clearly, the formation time $t = t_{QL}$ for the plateau $V_{\max} = (1.5-2.5)V_A$ is considerably shorter than the solar wind expansion time, $t_{QL}/t_{SW} = 0.01-0.3$ (we assumed an average $t_{SW} = 2.7 \times 10^5$ s). With these values, which cover typical proton nonthermal tails observed in the solar wind, the quasilinear diffusion process can be considered in the local approximation and our results are self-consistent. As the tail length approaches $3V_A$, the corresponding evolution timescale approaches t_{SW} for the shallowest spectra. This suggests that in average plasma conditions the tail length can hardly exceed $3V_A$, except when high turbulence levels are combined with shallow spectra.

In Figure 5 we are looking for the favorable conditions that facilitate the local production of nonthermal proton tails in the solar wind. To this end we fixed the plateau front at $V_{\max} = 1.5$ and plotted the corresponding formation time as function of V_{Tp}/V_A (which is proportional to the square root of the proton plasma beta). The spectral indexes are $p_2 = 2.5$,

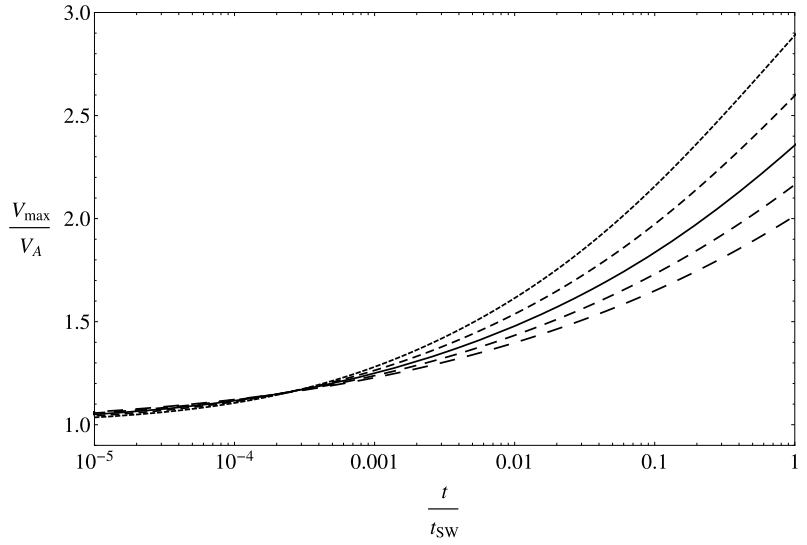

Figure 4 Normalized tail length $V_{\max}/V_{\rm A}$ as function of normalized time $t/t_{\rm SW}$. Spectral slopes are $p_2 =$ 2, 2.5, 3, 3.5, and 4 from the top curve to the bottom. All other plasma and turbulence parameters are the same for all curves (see text).

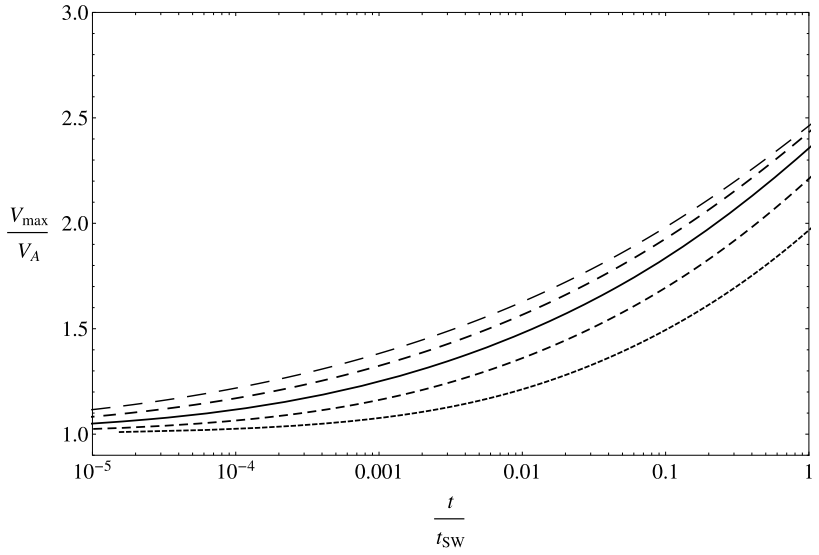

Figure 5 Formation time of the tail with $V_{\max} = 1.5V_{\rm A}$ as function of the proton thermal/Alfvén velocity ratio $V_{\rm Tp}/V_{\rm A}$ for the spectral slopes $p_2 = 2.5$, 3, 3.5, and 4 (from top to bottom). Other parameters are as in Figures 3 and 4.

3, 3.5, and 4 for the four curves from bottom to top. The most favorable $V_{\rm Tp}/V_{\rm A}$ for each curve is the one at which $t/t_{\rm SW}$ attains minimum. The shallowest spectra appeared to be most efficient at $V_{\rm Tp}/V_{\rm A} \simeq 1.5$, whereas the steepest spectra were most efficient at $V_{\rm Tp}/V_{\rm A} \lesssim 1$. These values are quite similar for all spectral slopes of interest, so that we can take as the

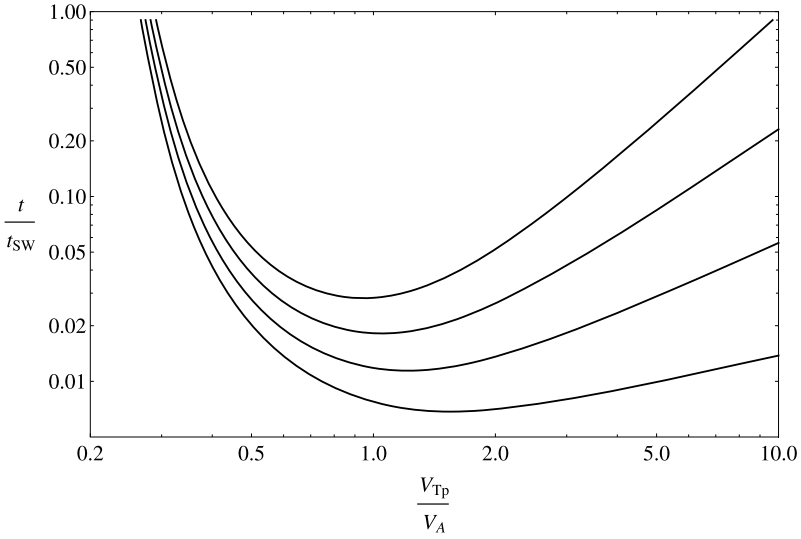

Figure 6 Normalized tail length $V_{\max}/V_{\rm A}$ as a function of normalized time $t/t_{\rm SW}$ for the same parameters as in Figure 4 except that the turbulence amplitudes are now adjusted by the scaling $W_{\mu 1} \propto p_2^{7.4}$. In this case the order of curves is reversed, $p_2 = 2$, 2.5, 3, 3.5, and 4 from bottom to top, which means the longer tails are generated by steeper spectra.

best-fit value $V_{\rm Tp}/V_{\rm A} \approx 1$, which is close to the average value in the solar wind at 1 AU. This means that the turbulence at 1 AU becomes more efficient in producing nonthermal tails.

In general, as is seen from Figures 4 and 5, the shallower kinetic spectra are more efficient in the tail production provided all other turbulence characteristics are fixed. However, not only the spectral slope, but also the level of turbulence is highly variable in the solar wind. Moreover, as was noticed by Smith *et al.* (2006), there is a positive correlation between the spectral flux before the spectral break and the spectral slope after it. The corresponding scaling in terms of spectral power can be written as $W_{\mu 1} \propto p_2^{7.4}$. Rescaling the turbulence amplitudes corresponding to $p_2 = 2$, 2.5, 3.5, and 4 slopes, we plot the resulting plateau front velocities for each p_2 in Figure 6. Now we obtain a reversed ordering of $V_{\max}$ with p_2, indicating that longer tails are generated by steeper spectra. Another new feature are the final values of $V_{\max}$, which are less scattered than in the case of uncorrelated amplitudes and slopes.

4.3. Numerical Example

At present, there are no data on the proton VDF and kinetic-scale turbulence measured simultaneously. The problem with the *Cluster* spacecraft is that they are capable of measuring the turbulence at sufficient frequency resolution, but the proton velocity-space resolution is insufficient in the solar wind conditions. It is nevertheless interesting to estimate a nonthermal proton tail that could result from a turbulence measured by *Cluster*.

In a particular case of *Cluster* measurements from 10 January 2004 from 06:15 to 06:25 UT, reported by Sahraoui *et al.* (2010), the background plasma parameters are $B_0 = 10.2$ nT, $n_0 = 16$ cm^{-3}, $T_{\rm e} = 10.4$ eV, $T_{\rm p} = 31$ eV, $V_{SW} = 548$ km s^{-1}, with the angle between the solar wind velocity and magnetic field $\theta_{BV} = 67^\circ$. Therefore, the proton thermal velocity in this case is about the same as the Alfvén velocity, $V_{\rm Tp} \simeq V_{\rm A} \simeq 55$ km s^{-1}, proton

cyclotron frequency $\Omega_p \simeq 0.94\ s^{-1}$, proton gyroradius $\rho_p \simeq 59$ km, and solar wind expansion time $t_{SW} = 76$ hours. The key turbulence characteristics are the spectral index at the proton kinetic scales $p = p_2 = 4$, the spectral break $\mu_1 = 0.4$, and the turbulence spectral density $W_{\mu 1} \simeq 0.15\ nT^2$ at $\mu = \mu_1$.

The dependence $V_{max}(t)$ for this case is plotted with the bottom line in Figure 4. One can observe that the turbulence should generate a nonthermal proton tail with $V_{max} \lesssim 2V_A$ at 1 AU. The proton VDF could not be measured by *Cluster*, but the average parallel energy of the protons was found to be higher than the perpendicular one, producing the effective temperature anisotropy $T_{p\parallel}/T_{p\perp} \lesssim 1.5$. This anisotropy cannot be produced by the quasilinear evolution of the initially isotropic Maxwellian VDF in the velocity range from V_A to $2V_A$. To obtain this anisotropy, one needs either more protons in the tail, or a longer tail ($V_{max} > 2V_A$), or both. The additional protons can be delivered to the tail by the nonlinear broadening of the Cherenkov resonance at $\mu \simeq \mu_1$, as given by Equation (22), and/or by the enhanced collisional diffusion at the steep velocity-space gradients at $V_z \simeq V_{min}$, where VDF undergoes a sharp transition from the Maxwellian VDF to the plateau-like. Most probably, both these processes have some effects on the tail density, and act synergetically. Again, we emphasize that the tail length is little affected by these processes. The longer tail can only be generated at shorter radial distances to the Sun, in more favorable conditions.

5. Conclusions and Discussion

We studied a Fokker–Planck proton diffusion in the solar wind induced by Alfvénic turbulence observed recently at proton kinetic scales (Sahraoui *et al.*, 2010; He *et al.*, 2011, 2012; Podesta and Gary, 2011; Salem *et al.*, 2012). Observations indicate that the turbulence is anisotropic and dominated by large perpendicular wavevectors, which is typical for KAWs possessing parallel electric fields and hence experiencing Cherenkov resonances. In the presence of a wide KAW spectrum with overlapping harmonics, the protons undergo numerous Cherenkov kicks resulting in a Fokker–Planck proton diffusion in the velocity space along the mean magnetic field.

We derived a quasilinear diffusion equation with the diffusion coefficient expressed in terms of measured turbulence parameters: spectral break wavenumber μ_1, turbulence amplitude $W_{\mu 1}$ at the spectral break, and spectral slopes p_2 below the break. At small and large μ, the asymptotic values for the spectral index are $p \simeq 1.7$ and 2.7, respectively (*e.g.* Alexandrova *et al.*, 2009). There is an intermediate spectral range, however, $\mu_1 < \mu < \mu_2$, where the spectrum slope is variable and often steepens to $p \simeq 3-4$ or even higher values (Sahraoui *et al.*, 2010). The turbulence power at these scales is mostly in form of weakly/mildly dispersive KAWs that are Cherenkov-resonant with protons in the velocity range covered by observed nonthermal tails, $V_z \simeq (1-3)V_A$. Enhanced nonlinear interaction among KAWs can explain these steep spectra in this range (Voitenko and De Keyser, 2011), but resonant generation of nonthermal tails can contribute to the steepening as well. On the other hand, an additional source for the KAW replenishing in the dissipation range can be provided by the nonlocal nonlinear coupling among KAWs and large-scale MHD AWs (Zhao, Wu, and Lu, 2011).

Rudakov *et al.* (2012) applied an asymptotic analysis to study the quasilinear proton diffusion in the strongly dispersive KAW turbulence with $\mu \gg 1$, which implies relatively high-energy resonant protons with $V_z \gg V_A$. However, this asymptotic analysis cannot be applied to typical tails with proton velocities $V_A < V_z < 3V_A$. The reason is that the KAW phase velocity (Equation (6)) cannot be approximated by a simple power-law dependence in

the resonant wavenumber range $0.3 < \mu < 3$. We focused on this tail-resonant range, where most of kinetic-scale power resides and where the full KAW dispersion (Equation (6)) has to be used. Consequently, the resulting diffusion equation is more complex and does not have an immediate analytical solution similar to that found by Rudakov *et al.* (2012). To proceed further analytically, we took into account a fast decrease of the diffusion coefficient with growing V_z (see Figure 2), which allowed us to formulate a simple yet plausible model for the quasilinear plateau, Equations (21) and (21), with the time-dependent front velocity $V_{\max}$ and height $f_{\rm pl}$. By using this model in the diffusion equation (Equations (18) and (19)), we found an analytical solution (Equation (24)) for the plateau-formation time as function of the plateau front velocity $V_{\max}$. Several numerical tests (one of them is shown in Figure 3) have confirmed the applicability of this model in solar wind conditions.

In general, our analysis and numerical estimations have revealed that the quasilinear proton diffusion driven by the observed solar wind turbulence provides a robust generation mechanism for nonthermal proton tails, which can explain that they are routinely observed in the solar wind. By implementing the measured characteristics of the turbulence at proton kinetic scales μ_1, $W_{\mu 1}$, and p_2 in our model, we estimated the timescale of the quasilinear plateau formation in the velocity space. For typical nonthermal tails with $V_{\max} = (1.5-2.5)V_{\rm A}$ the estimated formation time is $0.5-3$ h, which is much shorter than the solar wind expansion time at 1 AU. This indicates that the local generation of such tails observed in the solar wind is a natural consequence of the observed kinetic-scale Alfvén turbulence.

Some longer tails may require more time to develop, in which case a nonlocal radially-dependent problem has to be solved numerically using suitable solar wind models. In principle, with sufficient KAW power at $\mu > \mu_2$, the quasilinear plateau can extend well above $3V_{\rm A}$, where the asymptotic $\mu \gg 1$ analysis of Rudakov *et al.* (2012) can be applied. However, the turbulence level is usually insufficient to form the tails with $V_{\max} > 3V_{\rm A}$ within the required timescales, which is reflected in the fast growth of the formation time beyond $t_{\rm SW}$. This constraint is compatible with the rare observations of tails as long as this.

The most favorable conditions for tail generation in terms of $V_{\rm Tp}/V_{\rm A}$ occur in the range $V_{\rm Tp}/V_{\rm A} \simeq 1-1.5$ for spectral slopes ranging from $p_2 = 2.5$ to 4. The best-fit $(V_{\rm Tp}/V_{\rm A})_{\rm opt}$ does not vary much with the spectral slopes in the range of interest, and we can say that in general $(V_{\rm Tp}/V_{\rm A})_{\rm opt} \approx 1$. These conditions are often met at 1 AU. As is seen from Figure 5, the range of $V_{\rm Tp}/V_{\rm A}$ allowing for the tail generation has two bounds, upper $(V_{\rm Tp}/V_{\rm A})_{\rm cr2}$ and lower $(V_{\rm Tp}/V_{\rm A})_{\rm cr1}$. The upper bound $(V_{\rm Tp}/V_{\rm A})_{\rm cr2}$ is relatively high, its values for different spectral slopes are very scattered, and it is not very restrictive for the tail generation. In contrast, the lower bound $(V_{\rm Tp}/V_{\rm A})_{\rm cr1}$ is more restrictive. It has more concentrated values that are quite similar and are not so small, which is seen from Figure 5. For instance, for $V_{\max} \simeq 1.5V_{\rm A}$ tails $(V_{\rm Tp}/V_{\rm A})_{\rm cr1} \simeq 0.25$, and such tails cannot be generated locally if $V_{\rm Tp}/V_{\rm A} < 0.25$. The range of favorable $V_{\rm Tp}/V_{\rm A}$ cannot be extended toward lower values. Apparently, only short tails with $V_{\max} < 1.5V_{\rm A}$ can be generated at $V_{\rm Tp}/V_{\rm A} \approx 0.1$. Relatively long tails are expected with steep spectral slopes p_2 that are positively correlated with turbulence levels.

We also analyzed the particular case reported by Sahraoui *et al.* (2010). We found that the measured turbulence can generate a nonthermal tail extending to $V_{\max} \lesssim 2V_{\rm A}$, but the proton number density in the tail is insufficient to explain the measured temperature anisotropy of the protons. We suggest that the nonlinear resonance broadening and enhanced collisional diffusion at $V_z \lesssim V_{\rm A}$ are important mechanisms that significantly increase the proton number density in the tail. Yet another possibility is that the longer tail that produces the higher measured anisotropy was generated at shorter radial distances. The related effects require a more detailed investigation.

In addition to the amplitude-related constraints mentioned above, the tail length and shape can also be constrained by plasma instabilities. Several instabilities can develop on the plateau-like proton tail, including the fast magnetosonic, parallel Alfvén-cyclotron (Rudakov *et al.*, 2012), and oblique Alfvén (Daughton and Gary, 1999; Voitenko and Goossens, 2003) instabilities. Although Daughton and Gary (1999) and Voitenko and Goossens (2003) studied instability driven by the bump-on-tail, its generation mechanism is related to the anomalous Doppler (proton-cyclotron) resonance and not to inverse Landau damping and hence is not restricted to the bump-on-tail but can also be efficient with plateau-like distributions. The cyclotron diffusion of tail protons, driven by these instabilities, can constrain tail lengths and produce the proton-cyclotron quasilinear plateau reported by Marsch and Tu (2001) and Marsch and Bourouaine (2011), or even produce the bump-on-tail features. In turn, the nonthermal proton tails and beams can re-emit KAWs (Daughton and Gary, 1999; Voitenko and Goossens, 2003; Wu, Chen, and Wu, 2012; Nariyuki, Hada, and Tsubouchi, 2012) and significantly modify the nonlinear evolution of the high-amplitude circularly-polarized Alfvén waves (Nariyuki, Hada, and Tsubouchi, 2009, 2012). The complex interplay of these processes requires more investigations.

Obtained analytical expressions for the proton diffusion coefficient can be incorporated in more sophisticated solar wind models that account for external forces (electric and gravity), and both the particle-particle (Coulomb) and the wave-particle (Cherenkov) interaction terms in the right-hand side of Equation (9). Because of their complexity, these models need to be solved numerically. Our preliminary simulation results demonstrate that the kinetic-scale Alfvénic turbulence can create such nonthermal tails in the proton VDFs at radial distances $\lesssim 20$ solar radii (see detailed descriptions of these simulations in our accompanying paper (Pierrard and Voitenko, 2013)).

We did not concern ourselves here with the bump-on-tail features (proton beams) that are often observed in the solar wind. These distributions have not been reproduced by the uniform quasilinear diffusion we studied. However, with a variable level of the turbulence launched from the solar wind base, the irregularity of the generated tail length can easily produce the bump-on-tail features by the time-of-flight effect. Namely, in a region of enhanced turbulence the high-velocity end of a dense nonthermal tail propagates faster than the bulk protons. As a consequence, at larger radial distances this proton population penetrates a more quiet region with a weaker tail and appears there as a bump on the tail. This mechanism is compatible with Helios observations of time-variable bumps on virtually persistent tails (Marsch *et al.*, 1982).

In conclusion, the appearance of nonthermal proton tails and beams in the solar wind is unavoidable in the presence of kinetic-scale Alfvénic turbulence with sufficient amplitude. There are several other generation mechanisms for proton beams and tails (see Introduction) that can compete with, or replace each other in varying solar wind conditions. More detailed statistical correlation studies are needed to distinguish among them and to find the dominant mechanism in the solar wind. It would be particularly interesting to investigate the correlations between the tail lengths and/or densities and the turbulence levels at kinetic scales.

Acknowledgements This research was supported by the Belgian Federal Science Policy Office (via IAP Programme, project P7/08 CHARM) and by the European Commission's FP7 Program (projects 263340 SWIFF, and 313038 STORM). We thank the referee for his/her constructive criticism that helped us to improve this paper.

References

Alexandrova, O., Saur, J., Lacombe, C., Mangeney, A., Mitchell, J., Schwartz, S.J., Robert, P.: 2009, *Phys. Rev. Lett.* **103**, 165003.
Araneda, J.A., Marsch, E., Vinas, A.F.: 2008, *Phys. Rev. Lett.* **100**, 125003.
Borovsky, J.E., Gary, S.P.: 2011, *J. Geophys. Res.* **116**, A07110.
Chandran, B., Li, B., Rogers, B.N., Quataert, E., Germashewski, K.: 2010, *Astrophys. J.* **720**, 503.
Cranmer, S., Matthaeus, W., Breech, B., Casper, J.: 2009, *Astrophys. J.* **702**, 1604.
Daughton, W., Gary, S.P.: 1999, *Astrophys. J.* **602**, 1604.
Galinsky, V.L., Shevchenko, V.I.: 2012, *Astrophys. J.* **602**, 1604.
Gogoberidze, G., Chapman, S.C., Hnat, B.: 2012, *Phys. Plasmas* **19**, 102310.
Goldreich, P., Sridhar, S.: 1995, *Astrophys. J.* **438**, 763.
Hasegawa, A., Chen, L.: 1976, *Phys. Fluids* **19**, 1924.
He, J., Marsch, E., Tu, C., Yao, S., Tian, H.: 2011, *Astrophys. J.* **731**, 85.
He, J., Tu, C., Marsch, E., Yao, S.: 2012, *Astrophys. J. Lett.* **745**, L8.
Hollweg, J.V., Isenberg, P.A.: 2002, *J. Geophys. Res.* **107**, 1147.
Howes, G.: 2011, *Astrophys. J.* **738**, 40.
Lamy, H., Pierrard, V., Maksimovic, M., Lemaire, J.: 2003, *J. Geophys. Res.* **108**, 1047.
Leamon, R.J., Smith, C.W., Ness, N.F., Wong, H.K.: 1999, *J. Geophys. Res.* **104**, 22331.
Li, X., Lu, Q., Chen, Y., Li, B., Xia, L.: 2010, *Astrophys. J. Lett.* **719**, L190.
Lie-Svendsen, O., Leer, E.: 2000, *J. Geophys. Res.* **105**, 35.
Markovskii, S.A., Vasquez, B.J., Smith, C.W.: 2008, *Astrophys. J.* **675**, 1576.
Marsch, E.: 1991, In: Schwenn, R., Marsch, E. (eds.) *Physics of the Inner Heliosphere, II*, Springer, Heidelberg, 45.
Marsch, E.: 2006, *Living Rev. Solar Phys.* 3(1). http://solarphysics.livingreviews.org/Articles/lrsp-2006-1/.
Marsch, E., Bourouaine, S.: 2011, *Ann. Geophys.* **29**, 2089.
Marsch, E., Tu, C.-Y.: 2001, *J. Geophys. Res.* **106**, 8359.
Marsch, E., Muehlhauser, K.-H., Schwenn, R., Rosenbauer, H., Pilipp, W., Neubauer, F.: 1982, *J. Geophys. Res.* **87**, 52.
Matteini, L., Hellinger, P., Landi, S., Travnicek, P.M., Velli, M.: 2011, *Space Sci. Rev.* **172**, 737.
Nariyuki, Y., Hada, T., Tsubouchi, K.: 2009, *J. Geophys. Res.* **114**, A07104.
Nariyuki, Y., Hada, T., Tsubouchi, K.: 2012, *Phys. Plasmas* **19**, 082317.
Osmane, A., Hamza, A.M., Meziane, K.: 2010, *J. Geophys. Res.* **115**, A05101.
Pierrard, V., Lazar, M., Schlickeiser, R.: 2011, *Solar Phys.* **269**, 421.
Pierrard, V., Maksimovic, M., Lemaire, J.: 1999, *J. Geophys. Res.* **104**, 17021.
Pierrard, V., Voitenko, Y.: 2010, In: Maksimovic, M., Issautier, K., Meyer-Vernet, N., Moncuquet, M., Pantellini, F. (eds.) *Twelfth International Solar Wind Conference*, *AIP Conf. Proc.* **1216**, 102.
Pierrard, V., Voitenko, Y.: 2013, *Solar Phys.* doi:1007/s11207-013-0294-8.
Podesta, J.J., Gary, S.P.: 2011, *Astrophys. J.* **734**, 15.
Rudakov, L., Mithaiwala, M., Ganguli, G., Crabtree, C.: 2011, *Phys. Plasmas* **18**, 012307.
Rudakov, L., Crabtree, C., Ganguli, G., Mithaiwala, M.: 2012, *Phys. Plasmas* **19**, 042704.
Sahraoui, F., Goldstein, M.L., Belmont, G., Canu, P., Rezeau, L.: 2010, *Phys. Rev. Lett.* **105**, 131101.
Salem, C.S., Howes, G.G., Sundkvist, D., Bale, S.D., Chaston, C.C., Chen, C.H.K., Mozer, F.S.: 2012, *Astrophys. J. Lett.* **745**, L9.
Schekochihin, A.A., Cowley, S.C., Dorland, W., Hammett, G.W., Howes, G.G., Quataert, E., Tatsuno, T.: 2009, *Astrophys. J. Suppl.* **182**, 310.
Smith, C.W., Hamilton, K., Vasquez, B.J., Leamon, R.J.: 2006, *Astrophys. J. Lett.* **645**, L85.
Tu, C.-Y., Wang, L.-H., Marsch, E.: 2002, *J. Geophys. Res.* **107**, 1291.
Valentini, F., Perrone, D., Veltri, P.: 2011, *Astrophys. J.* **739**, 54.
Vocks, C., Mann, G.: 2009, *Astron. Astrophys.* **502**, 325.
Voitenko, Yu.M.: 1998, *Solar Phys.* **182**, 411.
Voitenko, Y., De Keyser, Y.: 2011, *Nonlinear Process. Geophys.* **18**, 587.
Voitenko, Y., Goossens, M.: 2002, *Solar Phys.* **209**, 37.
Voitenko, Y., Goossens, M.: 2003, *Space Sci. Rev.* **107**, 387.
Voitenko, Y., Goossens, M.: 2006, *Space Sci. Rev.* **122**, 255.
Wu, D.J., Chen, L., Wu, C.S.: 2012, *Phys. Plasmas* **19**, 024511.
Zhao, J.S., Wu, D.J., Lu, J.Y.: 2011, *Phys. Plasmas* **18**, 032903.